$Ca_V3.1$ is a tremor rhythm pacemaker in the inferior olive

Young-Gyun Park[a,1], Hye-Yeon Park[a,1], C. Justin Lee[b], Soonwook Choi[b,c], Seonmi Jo[a], Hansol Choi[a], Yang-Hann Kim[d], Hee-Sup Shin[b], Rodolfo R. Llinas[c,2], and Daesoo Kim[a,2]

[a]Department of Biological Sciences, Korea Advanced Institute of Science and Technology, Daejeon 305-701, Korea; [b]Center for Neural Science, Division of Life Science, Korea Institute of Science and Technology, Seoul 136-791, Korea; [c]Department of Physiology and Neuroscience, New York University School of Medicine, New York, NY 10016; and [d]Center for Noise and Vibration Control, Department of Mechanical Engineering, Korea Advanced Institute of Science and Technology, Daejeon 305-701, Korea

Edited by Edward G. Jones, University of California, Davis, CA, and approved May 3, 2010 (received for review March 8, 2010)

The rhythmic motor pathway activation by pacemaker neurons or circuits in the brain has been proposed as the mechanism for the timing of motor coordination, and the abnormal potentiation of this mechanism may lead to a pathological tremor. Here, we show that the potentiation of $Ca_V3.1$ T-type Ca^{2+} channels in the inferior olive contributes to the onset of the tremor in a pharmacological model of essential tremor. After administration of harmaline, 4- to 10-Hz synchronous neuronal activities arose from the IO and then propagated to cerebellar motor circuits in wild-type mice, but those rhythmic activities were absent in mice lacking $Ca_V3.1$ gene. Intracellular recordings in brain-stem slices revealed that the $Ca_V3.1$-deficient inferior olive neurons lacked the subthreshold oscillation of membrane potentials and failed to trigger 4- to 10-Hz rhythmic burst discharges in the presence of harmaline. In addition, the selective knockdown of $Ca_V3.1$ gene in the inferior olive by *sh*RNA efficiently suppressed the harmaline-induced tremor in wild-type mice. A mathematical model constructed based on data obtained from patch-clamping experiments indicated that harmaline could efficiently potentiate $Ca_V3.1$ channels by changing voltage-dependent responsiveness in the hyperpolarizing direction. Thus, $Ca_V3.1$ is a molecular pacemaker substrate for intrinsic neuronal oscillations of inferior olive neurons, and the potentiation of this mechanism can be considered as a pathological cause of essential tremor.

subthreshold oscillation | T-type calcium channel | harmaline

Low-threshold voltage-dependent Ca^{2+} channels (T-type) have been implicated in the generation of physiological and pathophysiological rhythms in the brain (1–3). In response to hyperpolarizing events, T-type Ca^{2+} channels are activated to induce low-threshold Ca^{2+} spikes (LTS) (4, 5), which are involved in the generation of neuronal oscillations, resonance, and pacemaker activities (1–3). Physiological and genetic studies have well demonstrated that T-type Ca^{2+} channels are involved in the generation of sleep oscillations and spike-and-wave discharges (SWDs) in the thalamocortical pathway, which relays sensory information to the cortex (1–3).

T-type Ca^{2+} channels are also highly expressed in cerebellar motor circuits (6), including inferior olive (IO), cerebellar Purkinje cells (PC), and deep cerebellar nuclei (DCN), which are known to relay information related to muscle coordination and balance (7, 8). Physiological and pharmacological studies have suggested that T-type Ca^{2+} channels play a role in the control of intrinsic oscillatory properties of IO neurons (9, 10). Considering that IO neurons receive both motor command and sensory information from the motor cortex and muscles, respectively, and provide the major afferent to the cerebellar motor pathway (7), it has been hypothesized that the oscillation of IO neurons could control the timing of muscle contractions (11). Consistent with this idea, lesions in the IO are known to cause severe motor abnormalities (12), but the specific role of IO rhythms at behavioral level remains to be demonstrated.

Here, we explore the role of $Ca_V3.1$ gene in olivocerebellar pathways and found that the potentiation of $Ca_V3.1$ channels in IO neurons plays a critical role in the generation of 4- to 10-Hz tremor-related rhythms and behavioral tremor in vivo.

Results

Mice Lacking $Ca_V3.1$ Are Selectively Resistant to the Harmaline-Induced Tremor. For insights into the role of $Ca_V3.1$ in motor functions, we first examined the motor-related capacity of $Ca_V3.1^{-/-}$ mice by using a number of behavioral experiments. In open field test, $Ca_V3.1^{-/-}$ mice showed a transient hyperactivity when first exposed to the test box, although they were eventually habituated as measured by normal baseline locomotor activities (Fig. 1*A*). However, the mice showed no other significant differences in overall motor capacity, including motor learning (Fig. 1*B*) and motor coordination of limbs during walking (Fig. 1 *C* and *D*), when compared with wild type. These findings suggest that $Ca_V3.1^{-/-}$ mice had no significant defects in motor learning and motor coordination, which has been associated with cerebellar motor functions and spinal reflexes (13). These findings suggested that the knockout of $Ca_V3.1$ gene causes no severe defects in physiological motor functions of mice.

Thus, we tried to examine the conditional phenotype induced by drugs that are known to disrupt motor coordination by inducing tremor, including oxotremorline, an agonist of muscarinic cholinergic receptors, for inducing 4- to 10-Hz resting tremor (14); physostigmine, an acetylcholinesterase inhibitor, for tremor with broad band frequencies (15); penitrem-A for 3- to 4-Hz action tremor (16); and harmaline for 5- to 14-Hz action tremor (14, 17, 18). Though $Ca_V3.1^{-/-}$ mice showed robust tremor activities when administered oxotremorine, physostigmine, or penitrem-A (Fig. 1*E*), these animals showed remarkably lower tremor activities than wild-type controls in response to harmaline (i.p. injection at 9 mg/kg; Movie S1), as measured by a decrease in the power (Fig. 1 *F* and *G*) and duration (Fig. 1*H*) of the tremor. Thus, this finding is consistent with the fact that those pharmacological tremor models are associated with different mechanisms (14–16) and suggests that $Ca_V3.1$ channels are indeed specifically associated with the harmaline-induced tremor.

Author contributions: Y.-G.P., H.-Y.P., C.J.L., R.R.L., and D.K. designed research; Y.-G.P., H.-Y.P., and S.C. performed research; Y.-G.P., H.-Y.P., C.J.L., S.J., Y.-H.K., and H.-S.S. contributed new reagents/analytic tools; Y.-G.P., H.-Y.P., C.J.L., S.C., and H.C. analyzed data; and Y.-G.P., H.-Y.P., R.R.L., and D.K. wrote the paper.

The authors declare no conflict of interest.

This article is a PNAS Direct Submission.

[1]Y.-G.P. and H.-Y.P. contributed equally to this work.

[2]To whom correspondence may be addressed. E-mail: daesoo@kaist.ac.kr or rodolfo.llinas@med.nyu.edu.

This article contains supporting information online at www.pnas.org/lookup/suppl/doi:10.1073/pnas.1002995107/-/DCSupplemental.

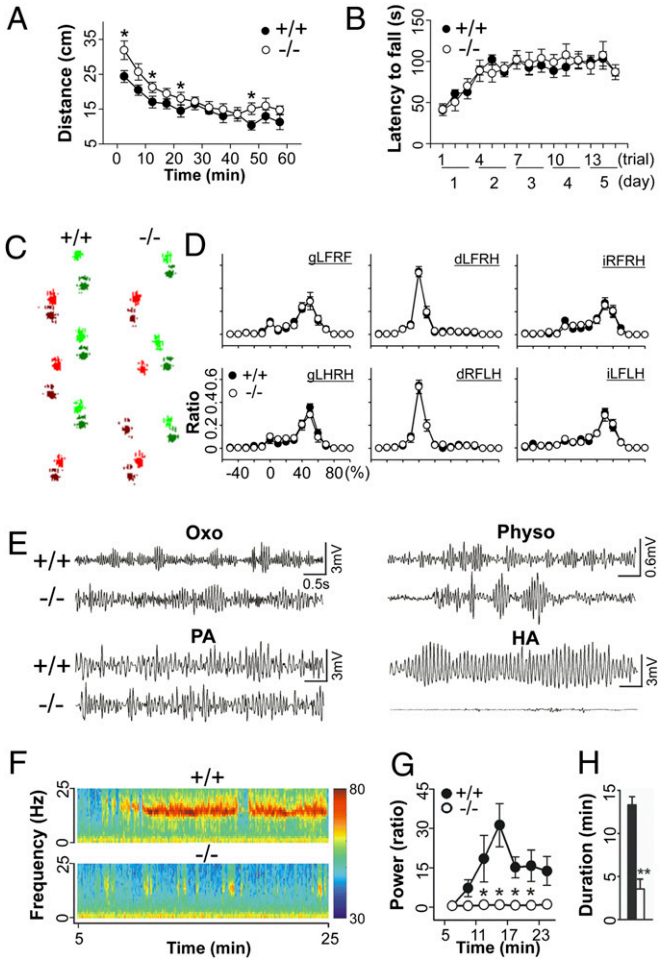

Fig. 1. Resistance of $Ca_V3.1^{-/-}$ mice to harmaline-induced tremor. (*A*) $Ca_V3.1^{-/-}$ animals have no significant locomotor defects on an open field test; mutant mice were hyperactive when first introduced to the open field. Two-way repeated ANOVA for genotype and time, $F(1, 131) = 10.063$, $^*P < 0.001$. ($^{+/+}$, $n = 7$; $^{-/-}$, $n = 7$). (*B*) Rotarod test. Motor coordination and learning was intact in $Ca_V3.1^{-/-}$ mice. Two-way repeated ANOVA for genotype and time, $F(1, 238) = 0.0387$, $P > 0.05$. ($^{+/+}$, $n = 10$; $^{-/-}$, $n = 9$). (*C*) Walking footprint patterns of two genotypes. Each paw of mice was marked by different colors: light red, left front paw; dark red, left hind paw; light green, right front paw; dark green, right hind paw. (*D*) Phase dispersion: temporal relationship between the placements of two paws within a step cycle of the walking pattern. d, diagonal; g, girdle; i, ipsilateral; LF, left front paw; RF, right front paw; LH, left hind paw; RH, right hind paw (e.g., gLFRF describes the relationship between the left front and right front paws). No significant difference was observed, χ^2 test, $P > 0.2$ ($^{+/+}$, $n = 5$; $^{-/-}$, $n = 6$) (*E*) Tremor induced by drugs: oxotremorine (Oxo) at 0.3 mg/kg; physostigmine (Physo) at 0.5 mg/kg; penitrem-A (PA) at 1.5 mg/kg; harmaline (HA) at 9 mg/kg. (*F*) Power spectral analysis of tremor induced by harmaline: color-coded power spectrum. Red-to-blue color means a variation in the intensity of tremors from 30 to 80 dB. (*G*) Comparison of harmaline-induced tremor activity between genotypes as measured by relative changes of tremor power (10–18 Hz) when compared with baseline. Two-way repeated ANOVA for genotype and time, $F(1, 54) = 8.506$, $^*P < 0.02$ ($^{+/+}$, $n = 7$; $^{-/-}$, $n = 6$). (*H*) Duration of the harmaline-induced tremor. Two-tailed *t* test, $^{**}P < 0.001$ ($^{+/+}$, $n = 7$; $^{-/-}$, $n = 6$). Error bars indicate SEM.

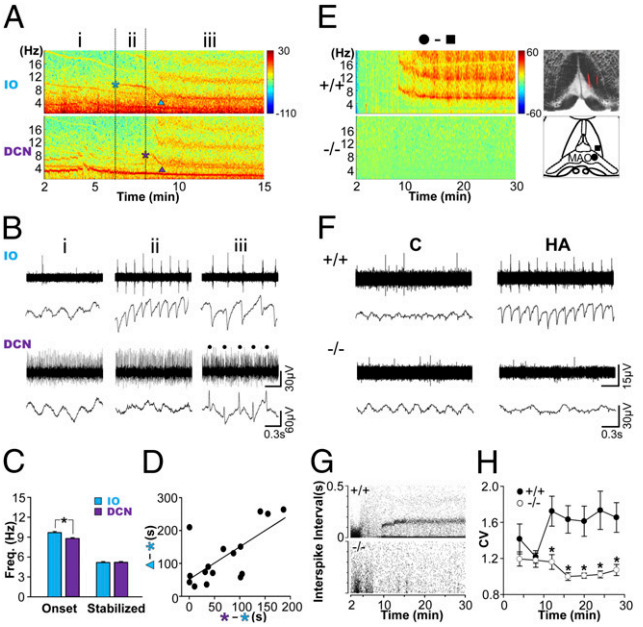

Fig. 2. Absence of harmaline-induced tremor-related oscillations in $Ca_V3.1^{-/-}$ mice. (*A*) Power spectral analysis of LFP obtained from simultaneous recordings in the IO and DCN after harmaline injection. Time sections are marked as before the onset of the oscillations (*i*), after the onset of the IO oscillations (*ii*), and after the onset of the DCN oscillations (*iii*). Fundamental oscillations are marked by asterisks, whereas other oscillations with higher frequencies are their harmonics. ▲, the time at which the frequency of the oscillation was stabilized. (*B*) Multiunit spike (*Upper*) and LFP (*Lower*) recordings in the IO and the DCN after harmaline injection. The rhythmic silencing of tonic spikes in DCN neurons, which is known as an effect of the inhibitory inputs from the Purkinje cells (19), is marked by dots. (*C*) Frequency of the oscillation at its onset or after stabilization. Two-tailed *t* test, $^*P < 0.05$ ($n = 16$). (*D*) Positive correlation between the stabilization latency of IO oscillations (*y* axis) and the onset time delay of the DCN oscillation (*x* axis). Linear regression, $R^2 = 0.478$; two-tailed *t* test, $P < 0.005$ ($n = 16$). (*E*) Representative LFP spectrograms in wild-type and $Ca_V3.1^{-/-}$ IO neurons. (*Left*) Electrode tracks are marked by red fluorescence (*Upper Right*). Diagram for the location of the electrode tip, inside (●) and outside (▲) of the medial and dorsal accessory olivary nuclei (MAO and DAO). (*Lower Right*) Subtracted power spectral densities between the inside and the outside of the MAO and DAO (see also Fig. S2). (*F*) Comparison of IO neuron multiunit and LFP activities between genotypes, 2 min (C) or 14 min (HA) after harmaline injection. (*G*) Opposite effect of harmaline on the interspike interval (ISI) of two genotypes. (*H*) The synchrony of spikes measured by coefficient of variance (CV) was compared between the genotypes. Two-way repeated ANOVA for genotype and time, $F(1, 104) = 11.575$, $^*P < 0.05$ ($^{+/+}$, $n = 13$; $^{-/-}$, $n = 7$). Error bars represent SEM.

$Ca_V3.1^{-/-}$ Mice Lack 4- to 10-Hz Harmaline-Induced Oscillations Initiated from the Inferior Olive. The main neuronal target affected by the null mutation of $Ca_V3.1$ gene was determined by examining harmaline-induced oscillations in mice. Because harmaline is known to induce 4- to 10-Hz oscillation in olivocerebellar pathways (18, 19), we performed simultaneous recordings of local field potentials (LFP) and multiunit spikes in the IO and the DCN, which are the major input and output pathways, respectively, in cerebellar motor circuits (7, 8). After harmaline administration, 4- to 10-Hz rhythmic oscillations initially appeared in the IO before reaching the DCN (Fig. 2 *A* and *B* and Fig. S1*A*; paired *t* test, $P < 0.01$). The delay between the IO and DCN oscillation was dose dependant, such that at 15 mg/kg, the mean delay was 71.82 s ($n = 16$), and at 9 mg/kg, the mean delay was 311.75 s ($n = 5$). Moreover, subtraction of spectrogram recorded from the IO with that of neighboring non-IO regions, which are at least 300 μm apart from the IO, showed that the 4- to 10-Hz oscillations originated directly from the IO neurons (Fig. 2*E* and Fig. S2). These findings support the idea that IO neurons are dominantly involved in the onset of the harmaline-induced oscillations in vivo (18).

In addition, the oscillation frequency was stabilized from the initial ~10-Hz frequency to ~5 Hz in both the IO and the DCN (Fig. 2*C*; one-way repeated ANOVA for time, in IO, $F(1, 15) =$

881.385, $P < 0.001$; in DCN, $F(1, 15) = 424.059$, $P < 0.001$). The dampening frequency reflects the increasing size of the neuronal population being synchronized, as described previously (20). Moreover, the latency of frequency stabilization was positively correlated with the onset delay of the DCN oscillations (Fig. 2*D*). Thus, the increase in synchronization among IO neurons seems to be a critical factor for the onset of tremor-related rhythms and the propagation of these rhythms to the DCN.

In contrast, in $Ca_V3.1^{-/-}$ mice, harmaline did not induce the 4- to 10-Hz bands in either the IO (Fig. 2 *E–H*) or the DCN (Fig. S3). Though wild-type IO neurons generated highly synchronous rhythmic discharges that were phase locked to the 4- to 10-Hz oscillations, the rhythmic spiking activities and LFP oscillations of IO neurons were significantly lower in the $Ca_V3.1^{-/-}$ IO neurons (Fig. 2 *F–H*). The firing rate of $Ca_V3.1^{-/-}$ IO neurons decreased after harmaline administration (Fig. S4; one-way repeated ANOVA for time, $F(6, 29) = 27.415$, $P < 0.001$). Hence, the onset of rhythmic firings and synchronous oscillation of IO neurons require the $Ca_V3.1$ channels.

$Ca_V3.1^{-/-}$ IO Neurons Lack a Capacity to Generate Rhythmic Action Potentials in Response to Harmaline-Induced Hyperpolarization. Next, we examined how the intrinsic properties of IO neurons were affected by the null mutation of $Ca_V3.1$. Intracellular recordings in brainstem slices indicated that in $Ca_V3.1^{-/-}$ IO neurons, typical protocol for activating T-type Ca^{2+} channel cannot induce low-threshold Ca^{2+} spike (Fig. 3*B Left*), a well-known physiological marker of T-type Ca^{2+} channel activity (1, 4, 5). In addition, we found a remarkable difference in the generation of the sub-threshold oscillation (STO). Wild-type neurons exhibited STO at resting membrane potentials, the amplitude of which was increased in the presence of harmaline (Fig. 3*A Upper*). The augmented STO was eventually coupled with vigorous rhythmic action potentials at 4–10 Hz (Fig. 3*A Upper*), similar to the frequency range examined in vivo (Fig. 2 *D* and *H*). In contrast, the majority of $Ca_V3.1^{-/-}$ IO neurons showed no STO at resting membrane potential (Fig. 3 *A* and *E*; $^{+/+}$, 0.138 ± 0.038 V^2/Hz; $^{-/-}$, 0.008 ± 0.001 V^2/Hz, two-tailed *t* test, $^*P < 0.05$).

Consistently, the rhythmicity of spike activities before harmaline treatment, which reflects the presence of STO (21), was lower in the $Ca_V3.1^{-/-}$ than wild-type IO neuron (Fig. 3*C*). In addition, $Ca_V3.1^{-/-}$ IO neurons failed to trigger rhythmic spiking in the presence of harmaline (Fig. 3*A*). Harmaline induced the hyperpolarization of membrane potentials (Fig. 3 *A* and *B*), which is known to reverse the inactivation of T-type Ca^{2+} channels (1, 4, 22) in both genotypes without any quantitative differences (Fig. 3*D*). These findings reveal that $Ca_V3.1$ channels are involved in the generation of STO and STO-coupled rhythmic spiking of IO neuron in response to harmaline.

Knockdown of $Ca_V3.1$ Gene in the Inferior Olive Attenuates the Harmaline-Induced Tremor in C57BL/6J Mice. Because the $Ca_V3.1$ gene is also expressed in cerebellar Purkinje cells and the DCN, which also show tremor-related rhythmicity (18, 19), we examined the role of $Ca_V3.1$ expression in the IO in the tremorogenesis. Local infusion of lentivirus harboring $Ca_V3.1$-specific *sh*RNA into the IO neurons (Fig. 4*A* and Fig. S5) efficiently attenuated harmaline-induced tremor (Fig. 4 *B* and *D*). Postmortem protein blotting confirmed the knockdown of $Ca_V3.1$ proteins in the IO (Fig. 4*C*). In addition, the local infusion of mibefradil, a nonspecific T-type Ca^{2+} channel blocker, to the IO also reduced the harmaline-induced tremors of wild-type animals

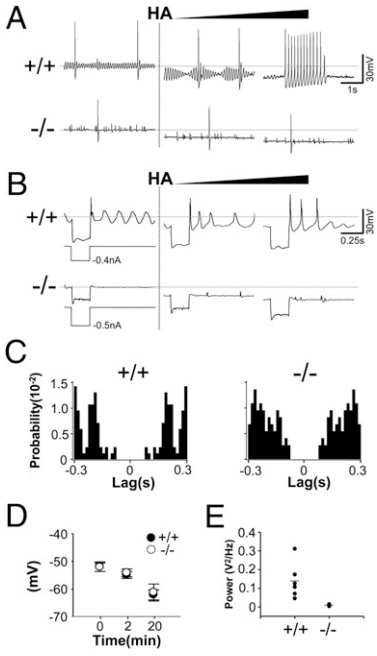

Fig. 3. Absence of STO and rhythmic burst discharges in $Ca_V3.1^{-/-}$ IO neurons. (*A*) In response to a continuous increase in harmaline concentration achieved by replacement of the bath medium with a 0.1 mg/mL harmaline solution, the amplitude of STO increased (*Center*, 5 min after) and then STO-coupled rhythmic burst discharges appears (*Right*, 7 min after) in wild type, but those effects are not examined in $Ca_V3.1^{-/-}$ IO neurons. (*B*) Rebound LTS induced by hyperpolarizing current inputs is augmented in the presence of harmaline, whereas no rebound LTS was elicited in $Ca_V3.1^{-/-}$ IO neurons. (*C*) Autocorrelogram of action potentials of IO neurons. Note the lowered rhythmicity of action potentials in $Ca_V3.1^{-/-}$ IO neurons. (*D*) Harmaline-induced hyperpolarization is not different between genotypes ($^{+/+}$, $n = 5$; $^{-/-}$, $n = 4$). (*E*) The power of STO is compared between genotypes ($^{+/+}$, $n = 6$; $^{-/-}$, $n = 6$). HA, harmaline administration. Error bars indicate SEM.

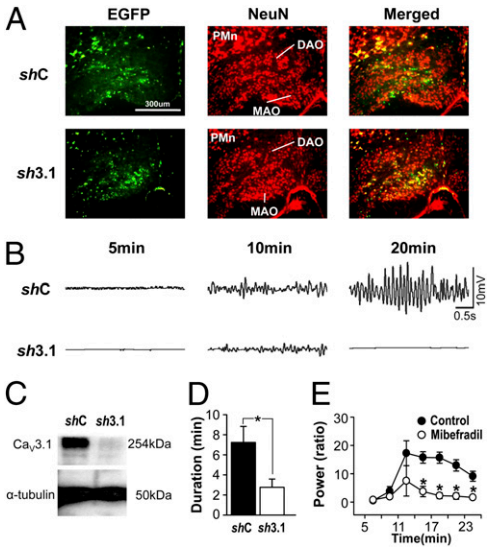

Fig. 4. Effect of IO $Ca_V3.1$ knockdown on the harmaline-induced tremor. (*A*) Immunostaining of brain slices for EGFP and NeuN proteins, for detecting infected cell and the soma of neurons, respectively. Approximately 40–50% of IO neurons are infected with lentivurses harboring either *sh*RNA-$Ca_V3.1$ (*sh*3.1) or control (*shC*). DAO, dorsal accessory olivary nucleus; MAO, medial accessory olivary nucleus; PMn, paramedian reticular nucleus. (*B*) Tremor activity induced by harmaline administration is decreased by *sh*RNA-$Ca_V3.1$. (*C*) Western blot analysis of $Ca_V3.1$ proteins isolated from infected IO regions by microdissection under microscope. (*D*) Duration of the harmaline-induced tremor. Two-tailed *t* test, $^*P < 0.05$ (*shC*, $n = 7$; *sh3.1*, $n = 12$). (*E*) The effect of the mibefradil in the IO on the harmaline-induced tremor. Two-way repeated ANOVA for genotype and time, $F(1, 42) = 24.674$, $^*P < 0.05$, saline, $n = 5$; mibefradil, $n = 5$. Error bars indicate SEM.

(Fig. 4*E*). These findings suggest that the $Ca_V3.1$ channels expressed in the IO were relevant for the tremorogenic action of harmaline.

Harmaline Modifies the Voltage-Dependent Responsiveness of $Ca_V3.1$ Channels. Given the findings described herein, we tried to address the effect of harmaline on the $Ca_V3.1$-dependent I_T. Voltage-clamp recording of IO neurons indicated that in a conventional protocol, which uses 20- to 40-mV hyperpolarization followed by depolarization for measuring the activation of I_T (4, 5), harmaline dose-dependently inhibited I_T in IO neurons (Fig. 5 *A* and *C* and Fig. S6). To avoid indirect effects that could result from the non-specific binding of harmaline on other ion channels (23) or an incomplete integrity of patch clamping due to well-developed electrical synapses of IO neurons (22), we measured I_T in HEK cells, which express $Ca_V3.1$ channels (HEK-$Ca_V3.1$). Consistently, HEK-$Ca_V3.1$ cells showed reduced I_T in the presence of harmaline, although the inhibitory effect was smaller when compared with that found in IO neurons (Fig. 5*C*). These findings suggest that harmaline directly modulates the activation of $Ca_V3.1$ channels.

Next, we examined the effect of harmaline on voltage dependence of $Ca_V3.1$ channels in HEK-$Ca_V3.1$ cells, because IO neurons have gap junctions that might cause $Ca_V3.1$-independent currents in IO neurons. In the plot of voltage dependence, both activation and inactivation curves were shifted toward negative potential in the presence of harmaline (Fig. 5*D*). The degree of shifting of both curves by harmaline were differential (Fig. 5*E*); In a range of 0.1 to 10 μM, the shifting of the activation curve (−mV) was linearly increased to increasing harmaline concentrations, but that of the inactivation curve was not significantly changed (Fig. 5*E*; one-way ANOVA, $P > 0.05$), suggesting that the activation effect of harmaline could be more dominant. Considering the voltage dependence of $Ca_V3.1$ channels, we quantified the effect of harmaline on membrane potentials (Fig. 5*F*). As previously described (9), harmaline dose-dependently hyperpolarizes the membrane potentials up to −60 to −70 mV, but more than 100 μM of harmaline was not effective at inducing more hyperpolarization (Fig. 5*F*).

Based on the complex action of harmaline on $Ca_V3.1$-dependant I_T, which seems to induce three different effects: inhibition of activation (Fig. 5 *A*–*C*), shifts of voltage dependency (Fig. 5 *D* and *E*), and induction of membrane potential hyperpolarization (Fig. 5*F*), we mathematically simulated the net influx of I_T in IO neuron in response to various types of variables, including the amplitude of hyperpolarizing prepulse, depolarizing pulse, and membrane hyperpolarization (Fig. S7). Results from this simulation showed that many types of inputs increased I_T at around 10 μM, but the same inputs inhibited I_T at 1 μM or 100 μM (Fig. 5*G*). In addition, negative currents input causing less than 20 mV hyperpolarization usually increased I_T, but that with larger than 20 mV hyperpolarization led to the suppression of these currents in 10 μM harmaline (Fig. 5*G*).

Consistent with our findings, voltage clamping of HEK-$Ca_V3.1$ showed that, in the presence of 10 μM harmaline, 5- to 15-mV hyperpolarizing prepulses increased I_T, but 20 mV led to the inhibition of I_T when compared with controls (Fig. 5*H* and Fig. S8). The hyperpolarization of more than 20 mV from the resting membrane potentials, however, may not be physiological because (*i*) almost all ions existing in naive neuron do not have reversal potential below −80 mV and (*ii*) many inward-rectifying potassium channels, which are also highly expressed in IO neurons (24), strongly depolarize membrane potential above −80 mV. Hence, these findings suggest that harmaline inhibits activation of $Ca_V3.1$ channels but can potentiate I_T through these channels in physiological conditions by modifying parameters related to the voltage-dependence responsiveness of these channels.

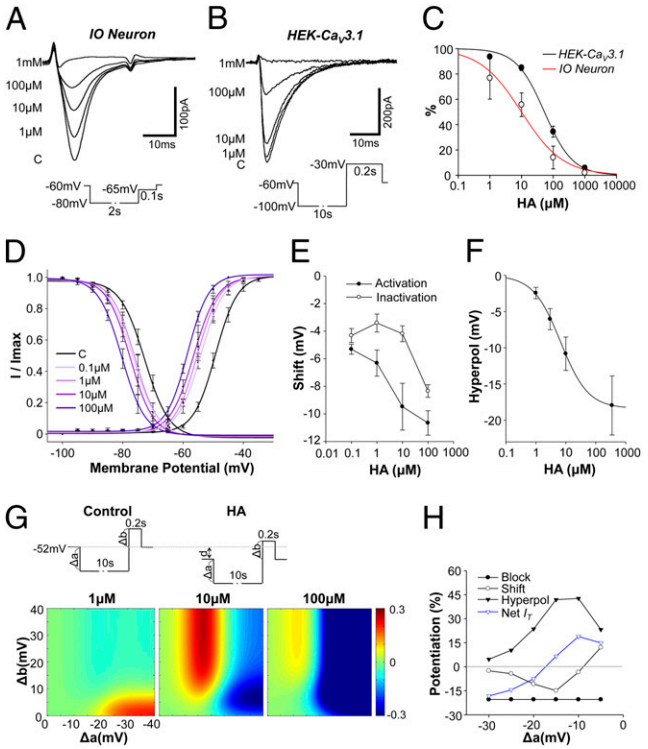

Fig. 5. Potentiation of $Ca_V3.1$ channels by harmaline. Dose-dependent inhibition of I_T activation by harmaline either in IO neurons (*A*) or in HEK-$Ca_V3.1$ cells (*B*). (*C*) Dose–response curve smoothed by fitting to the data with an exponential function. (*D*) Shifting inactivation and activation curves by harmaline. Curves are fitted result with Boltzmann equation. (*E*) Dose-dependent shifting of voltage dependence. (*F*) The amount of hyperpolarization of IO neurons in the presence of harmaline. (*G*) Computational modeling of the net I_T influx in response to stimuli. (*Upper*) I_T induction protocol consisting of hyperpolarizing prepulse (Δa), depolarizing inputs (Δb), and membrane potential hyperpolarization by harmaline (d). (*Lower*) Changing ratio of net I_T after harmaline treatment (1, 10, 100 μM) at various voltage steps. HA, after harmaline treatment. (*H*) Relative contribution of parameters to I_T in HEK-$Ca_V3.1$ cells after 10 μM harmaline. Block, inhibition of I_T activation; Shift, shifting voltage dependences of I_T; Hyperpol, harmaline-induced hyperpolarization.

Discussion

Essential tremor is the most frequent movement disorder characterized by the onset of tremor during voluntary movement; however, as the name implies, its pathology and etiology remains unknown (17, 25). Harmaline, a derivative of β-carboline found in brewed coffee (26), cigarettes (27), and blood of patients with essential tremor (28), induces essential-like tremor in animals and human (25, 28). Because it causes 4- to 10-Hz tremor rhythms in neurons that are associated with olivocerebellar pathway, harmaline has been used for the study of tremor rhythms in the brain (14, 17, 25).

The present study shows that the tremorogenic action of harmaline depends on $Ca_V3.1$ channels (Fig. 1) expressed in IO neurons (Figs. 2–4) and reveals the mechanism of action of this drug (Fig. 5). Although harmaline inhibits the activation of $Ca_V3.1$ channels, it could potentiate these channels by modulating other parameters: (*i*) differential shifting of activation and inactivation voltage dependence, expanding the window of membrane potentials where $Ca_V3.1$ channels can be potentiated; (*ii*) hyperpolarization of membrane potentials, leading to the optimal range of membrane potentials to potentiate these channels. Furthermore, the positive effects of harmaline are concentration dependent, and are maximized at around 10 μM of harmaline (Fig. 5). Consistently, the 10-μM range is known as an effective dose to

induce tremor in cerebrospinal fluids of mice (29) and evokes tremor rhythms in IO neurons in vivo (Fig. 2). Thus, our findings suggest that potentiation or inhibition of $Ca_V3.1$ channels can be a unique measure for searching pathological causes of tremor or therapeutic mechanisms of antitremor drugs, which have been largely unknown.

The present experimental paradigm also afforded a possible explanation of how the potentiation of $Ca_V3.1$ channels contributes to tremor (Fig. 1) and tremor-related rhythms in IO neurons (Fig. 2). One classical hypothesis is that the STO of IO neurons can synchronize neuronal activities via electrical synapses (9, 30); however, a previous study showed that mice lacking connexin-36, a major component of the electrical synapses of IO neurons, exhibited robust tremor activities when administered harmaline (30). This suggests that the electrical synapse is not the only mechanism underlying network oscillation.

Our present findings indicate that $Ca_V3.1^{-/-}$ mice lack the STO in IO neurons (Fig. 3) and that they are impaired in the generation of tremor-related rhythm (Fig. 2) and behavioral tremor (Figs. 1 and 4). These findings support the relevance of STO in the synchronization of IO neurons (9, 30, 31). Harmaline increases the amplitude of STO, and this leads to rhythmic burst spikes (Fig. 3), which may efficiently activate neighboring neurons via electrical and chemical synapses (9, 30, 32), thereby increasing the number of neurons being synchronized (Fig. 2 *A–D*). The synchronization of IO neurons may, eventually, lead to the 4- to 10-Hz tremor-related oscillations (Fig. 2).

It has been reported that the IO and DCN neurons are synchronized together when animals are administered harmaline (19). Our finding shows, however, that the onset of IO oscillations is always preceded by that of DCN (Fig. 2*A* and Fig. S1*A*), and the propagation of tremor-related rhythms to the DCN is also modulated by the number of IO neurons being synchronized (Fig. 2*D*). Moreover, the onset of IO oscillations coincides with the time of tremor onset, and that of DCN oscillations is found in the period when the intensity of tremor is increasing (Fig. S1*B*). Hence, the synchronization of IO neurons seems to be critical for the onset of behavioral tremor, and the following synchronization of DCN neurons may contribute to the increase of tremor strength and affected body parts.

Although our findings show a critical role of $Ca_V3.1$ channels in the generation of IO oscillations, other mechanisms also play important supporting functions in this oscillatory behavior (9, 33, 34); e.g., *Ih* currents were measured by depolarizing sacs in each genotype and it was found that $Ca_V3.1^{-/-}$ IO neurons have lower HCN channel activity (Fig. S9), which is consistent with previous findings that low-threshold calcium conductance leads to the persistent activation of *Ih* (35). Hence, this finding suggests that $Ca_V3.1$ channels could indirectly modulate HCN channels, which have been implicated in the oscillatory activities of IO neurons (33). It remains to be studied how other mechanisms can be associated with the potentiation of $Ca_V3.1$ channels.

Concerning the physiological significance of STO, it has been proposed that STO contributes to the timing of motor coordination (11), as IO neurons have been shown to relay peripheral sensory information back to the cerebellum (36) and function as a comparator in several motor-learning models (8, 37). However, we found no significant motor defects in $Ca_V3.1^{-/-}$ mice (Fig. 1), which have reduced capacity for generating intrinsic IO rhythms (Fig. 3). The relatively intact motor capacity of $Ca_V3.1^{-/-}$ mice can be due to physiological or developmental compensation, or that a more stringent test of motor timing may be required (31, 38). It is also plausible that STO is involved in higher motor functions that require faster processing of motor-related information (11), although this was not addressed in the present study. Detailed behavioral testing of mice with the $Ca_V3.1$ knocked down in adult IO neurons will provide clues concerning the function of STO.

The only notable difference found in $Ca_V3.1^{-/-}$ mice was that they showed a transient hyperactivity with normal habituation in open field test (Fig. 1*A*). Considering that the increased activity in the early period of the test reflects an emotional response of mice to novel environmental stimuli (39), this phenotype can be explained, in part, by the enhanced vigilance of $Ca_V3.1^{-/-}$ mice reported in previous studies; they show longer waking episodes during sleep (40) and resistance to GABA-B agonists, which cause a loss of consciousness (2). In the thalamocortical pathways, T-type Ca^{2+} channels are involved in the generation of low-threshold burst spikes during sleep and drowsiness (41), which contribute to the sensory gating mechanism (42). Hence, it is plausible that the absence of thalamic burst spikes facilitates the thalamocortical relay of sensory information on novel stimuli in $Ca_V3.1^{-/-}$ mice.

In conclusion, the present study supports the view that tremor-related oscillations in the olivocerebellar pathways are a neural signature for essential tremor (9, 19). It also suggests that $Ca_V3.1$ channels play a critical role in the onset of tremor-related rhythms. It follows, then, that $Ca_V3.1$ can be directly linked with essential tremor. For example, the kinetic component of essential tremor (17, 25) may be explained by the activation of these channels in IO, by sensory inputs generated by movement, which were known to be conducted into IO (37). Further investigation for conditions to potentiate $Ca_V3.1$ channels may provide clues on the cause of essential tremor and on novel drug targets for the disease. Beyond the issue of essential tremor, the role of IO rhythmicity modulated by $Ca_V3.1$ channels in higher motor functions (11) remains to be elucidated.

Methods

Drug-Induced Tremor. A mouse was placed in the test cage for 7 min, and one of the following tremorogenic drugs was injected i.p.: oxotremorine sesquifumarate (0.3 mg/kg), penitrem-A (1.5 mg/kg), or harmaline hydrochloride dihydrate (9 or 15 mg/kg). Tremor activity was measured by using DC accelerometer (DC Response Accelerometer, model 3711D1FA3G; Piezotronics) or ICP accelerometer (Integrated Circuit Piezoelectric Accelerometer, model 352C66; Piezotronics) attached to the bottom of the test cage, which was hung in the air by two elastic wires (Fig. S10 and Movie S1).

Electrophysiological Recording in Vivo. Male C57BL/6J mice (10–28 wk old) were fixed on a stereotaxic device under urethane anesthesia (1.65 g/kg). Body temperature of mice was monitored and maintained by a temperature controller (Homeothermic Blanket System; Harvard Apparatus). Quartz-coated tetrodes (0.5–2 MΩ; Thomas Recording) were placed either at the subdivision of the inferior olive [DAO and MAO; distance from bregma (in mm), −7.4, ± 0.5, 4.5–5.3: anterior-posterior (AP), mediolateral (ML), dorsal-ventral (DV) axes] or at the medial cerebellar nuclei (−6.4, ± 0.8, 2.0–2.6: AP, ML, DV), and harmaline (9 or 15 mg/kg) was injected i.p. To localize the site of the recordings, the tips of the tetrodes were briefly dipped in fluorescence dye solution (DiI, 50 mg/mL; Sigma) before tissue penetration, and electrode tracks in the brainstem slices were visualized under a confocal microscope using a rhodamine filter, as previously described (43). Signals were amplified using an AC amplifier (PGMA; Thomas Recording) and then sampled at 30 kHz (DT3010; Neuralynx) and filtered at either 480–6,000 Hz (for the measurement of multiunit activity) or 1.52–50 Hz (for the measurement of LFP).

Whole-Cell Patch-Clamp Recording. ***In HEK cells.*** $Ca_V3.1$-Kir2.1 transfected HEK cell line (44) were used in demonstrating harmaline effect to I_T. Borosilicate glass electrodes with a resistance of 3–4 MΩ were pulled and filled with internal solution containing (in mM): 130 CsCl, 4 $MgCl_2$, 10 Hepes, 5 TEA-Cl, 10 EGTA, 4 Mg-ATP, and 0.3 Na_2-GTP. I_T was recorded in external solution containing (in mM) 100 NaCl, 25 TEA-Cl, 3 KCl, 20 Hepes, 2 $MgCl_2$, and 5 $BaCl_2$. For holding potential, −60 mV was used.

In IO neurons. Preparing IO slices for patch-clamp recording were performed similarly to a previous study (30). $Ca_V3.1$ wild-type and knockout mice (postnatal day 12–15) were intracardially perfused with an ice-cold solution containing (in mM) 124 sucrose, 3 KCl, 1.25 NaH_2PO_4, 2 $MgSO_4$, 26 $NaHCO_3$, 10 dextrose, and 2 $CaCl_2$. The brain was then rapidly removed, and slices (350 μm thick) were made with a vibratome. After incubation for at least 45 min in 32 °C, slices were kept at room temperature in a holding chamber until they

were transferred to a submersion-type recording chamber held at 32 °C. Solution used for slice incubation contained 126 NaCl, 3 KCl, 1.25 NaH_2PO_4, 2 $MgSO_4$, 26 $NaHCO_3$, 10 dextrose, and 2 $CaCl_2$, saturated with 95% O_2/5% CO_2; the recording solution was the same, except for reduced divalent ion levels (1 $MgSO_4$ and 1 $CaCl_2$) and a slight increase in potassium (3.5 KCl). Recording pippet (4-7 MΩ) were filled with (in mM) 115 CsOH, 115 D-gluconic acid, 10 Hepes, 0.5 EGTA, 4 Mg-ATP, 0.3 GTP-Tris, 7 PC-Tris, 2 NaCl, 20 TEA-Cl, and 2 $MgCl_2$. After rupturing, IO neurons were maintained at −60 mV, and recording solution was substituted with Ca^{2+} current recording solution, which is composed of (in mM) 66 NaCl, 3.5 KCl, 1.25 NaH_2PO_4, 1.3 $MgSO_4$, 26 $NaHCO_3$, 10 dextrose, 2.5 $CaCl_2$, 60 TEA-Cl, 5 4-aminopyridine, 3 CsCl, 0.0125 bicuculline methiodide, and 0.001 tetrodotoxin. Because of high C_m value of IO neurons (80–130 pF) and presence of gap junctions, which cause incomplete voltage clamping, we also recorded in $Ca_V3.1$ wild-type and mutant IO neuron and confirmed that current induced by the voltage step is $Ca_V3.1$ current (Fig. S6). Signals were amplified by Multiclamp 700B or Axopatch 200B (Axon Instrument) and digitized by Digidata 1322A (Axon Instruments). Cells were visualized by Ixon camera (Andor).

Computational Modeling of I_T. I_T has been known to be activated only after the deinactivation, a process of recovery from inactivation by hyperpolarizing prepulse (4, 5). Thus, the amplitude of I_T by $Ca_V3.1$ can be determined by the following function,

$$T_{\text{control}} = fi(r_m - a) * fa(r_m + b),$$

where r_m is the IO neuron resting membrane potential, a and b are the degree of hyperpolarizing/depolarizing voltage step sequence (Fig. 5*F Left*), f_i is the ratio of recovered channels from inactivation (Fig. S7*A*), and f_a is the current amplitude resulting from depolarizing pulse normalized with the maximal current before harmaline treatment (Fig. S7*B*).

Because harmaline shifts both inactivation and activation curve and induces membrane potential hyperpolarization, amplitude of net I_T after harmaline treatment can be described with a slightly different equation:

$$T_{\text{harmaline}} = g_i(r_m - d - a) * g_a(r_m - d + b),$$

where d is the level of preconditioned membrane potential hyperpolarization (Fig. 5*F*) and g_i and g_a are the shifted inactivation and activation curve, respectively, at certain harmaline concentration. For calculating g_i, the ratio of channels recovered from inactivation after harmaline is calculated by normalizing inactivation curve with the percentage of current remaining at a given harmaline concentration (Fig. 5*C*).

ACKNOWLEDGMENTS. D. K. thanks Walton Jones for critical comments on our manuscript. Y.G. thanks Boeun Yoon for helping with the voltage-clamp experiment. We thank Dr. Dong-jin Kim for approving the use of HEK-CaV3.1 cell line. This work was supported by the Biotechnology Development Program of the Korea Ministry of Education, Science and Technology Grants R01-2006-000-10799-0, M10748000345-08N4800-34510, and 20090083354 (to D.K.) and by National Institutes of Health Grant NS13742 (to R.R.L.).

1. Huguenard JR (1996) Low-threshold calcium currents in central nervous system neurons. *Annu Rev Physiol* 58:329–348.
2. Kim D, et al. (2001) Lack of the burst firing of thalamocortical relay neurons and resistance to absence seizures in mice lacking alpha(1G) T-type Ca(2+) channels. *Neuron* 31:35–45.
3. McCormick DA, Bal T (1997) Sleep and arousal: Thalamocortical mechanisms. *Annu Rev Neurosci* 20:185–215.
4. Crunelli V, Lightowler S, Pollard CE (1989) A T-type Ca2+ current underlies low-threshold Ca2+ potentials in cells of the cat and rat lateral geniculate nucleus. *J Physiol* 413:543–561.
5. Perez-Reyes E (2003) Molecular physiology of low-voltage-activated t-type calcium channels. *Physiol Rev* 83:117–161.
6. Talley EM, et al. (1999) Differential distribution of three members of a gene family encoding low voltage-activated (T-type) calcium channels. *J Neurosci* 19:1895–1911.
7. Apps R, Garwicz M (2005) Anatomical and physiological foundations of cerebellar information processing. *Nat Rev Neurosci* 6:297–311.
8. Wolpert D, Miall R, Kawato M (1998) Internal models in the cerebellum. *Trends Cogn Sci* 2:338–347.
9. Llinás R, Yarom Y (1986) Oscillatory properties of guinea-pig inferior olivary neurones and their pharmacological modulation: An in vitro study. *J Physiol* 376:163–182.
10. Lampl I, Yarom Y (1997) Subthreshold oscillations and resonant behavior: Two manifestations of the same mechanism. *Neuroscience* 78:325–341.
11. Welsh JP, Lang EJ, Suglhara I, Llinás R (1995) Dynamic organization of motor control within the olivocerebellar system. *Nature* 374:453–457.
12. Llinás R, Walton K, Hillman DE, Sotelo C (1975) Inferior olive: Its role in motor learing. *Science* 190:1230–1231.
13. Brooks SP, Dunnett SB (2009) Tests to assess motor phenotype in mice: A user's guide. *Nat Rev Neurosci* 10:519–529.
14. Wilms H, Sievers J, Deuschl G (1999) Animal models of tremor. *Mov Disord* 14: 557–571.
15. Sarkar S, Thomas B, Muralikrishnan D, Mohanakumar KP (2000) Effects of serotoninergic drugs on tremor induced by physostigmine in rats. *Behav Brain Res* 109:187–193.
16. Cavanagh JB, et al. (1998) The effects of the tremorgenic mycotoxin penitrem A on the rat cerebellum. *Vet Pathol* 35:53–63.
17. LeDoux MS, ed (2005) *Animal Models of Movement Disorders* (Academic, San Diego).
18. Llinás R, Volkind RA (1973) The olivo-cerebellar system: Functional properties as revealed by harmaline-induced tremor. *Exp Brain Res* 18:69–87.
19. de Montigny C, Lamarre Y (1973) Rhythmic activity induced by harmaline in the olivo-cerebello-bulbar system of the cat. *Brain Res* 53:81–95.
20. Schnitzler A, Gross J (2005) Normal and pathological oscillatory communication in the brain. *Nat Rev Neurosci* 6:285–296.
21. Khosrovani S, Van Der Giessen RS, De Zeeuw CI, De Jeu MT (2007) In vivo mouse inferior olive neurons exhibit heterogeneous subthreshold oscillations and spiking patterns. *Proc Natl Acad Sci USA* 104:15911–15916.
22. Llinás R, Yarom Y (1981) Electrophysiology of mammalian inferior olivary neurones in vitro. Different types of voltage-dependent ionic conductances. *J Physiol* 315: 549–567.
23. Splettstoesser F, Bonnet U, Wiemann M, Bingmann D, Büsselberg D (2005) Modulation of voltage-gated channel currents by harmaline and harmane. *Br J Pharmacol* 144: 52–58.
24. Karschin C, Dissmann E, Stühmer W, Karschin A (1996) IRK(1-3) and GIRK(1-4) inwardly rectifying K+ channel mRNAs are differentially expressed in the adult rat brain. *J Neurosci* 16:3559–3570.
25. Elble RJ (1996) Central mechanisms of tremor. *J Clin Neurophysiol* 13:133–144.
26. Pfau W, Skog K (2004) Exposure to beta-carbolines norharman and harman. *J Chromatogr B Analyt Technol Biomed Life Sci* 802:115–126.
27. Herraiz T (2002) Identification and occurrence of the bioactive beta-carbolines norharman and harman in coffee brews. *Food Addit Contam* 19:748–754.
28. Louis ED, et al. (2002) Elevation of blood beta-carboline alkaloids in essential tremor. *Neurology* 59:1940–1944.
29. Robertson HA (1980) Harmaline-induced tremor: The benzodiazepine receptor as a site of action. *Eur J Pharmacol* 67:129–132.
30. Long MA, Deans MR, Paul DL, Connors BW (2002) Rhythmicity without synchrony in the electrically uncoupled inferior olive. *J Neurosci* 22:10898–10905.
31. Leznik E, Llinás R (2005) Role of gap junctions in synchronized neuronal oscillations in the inferior olive. *J Neurophysiol* 94:2447–2456.
32. Placantonakis DG, Bukovsky AA, Zeng XH, Kiem HP, Welsh JP (2004) Fundamental role of inferior olive connexin 36 in muscle coherence during tremor. *Proc Natl Acad Sci USA* 101:7164–7169.
33. Bal T, McCormick DA (1997) Synchronized oscillations in the inferior olive are controlled by the hyperpolarization-activated cation current I(h). *J Neurophysiol* 77: 3145–3156.
34. Lamarre Y (1995) Central mechanisms of experimental tremor and their clinical relevance. *Handbook of Tremor Disorders* (Dekker, New York), pp 103–118.
35. Lüthi A, McCormick DA (1998) Periodicity of thalamic synchronized oscillations: The role of Ca2+-mediated upregulation of Ih. *Neuron* 20:553–563.
36. de Zeeuw CI, Holstege JC, Ruigrok TJ, Voogd J (1989) Ultrastructural study of the GABAergic, cerebellar, and mesodiencephalic innervation of the cat medial accessory olive: Anterograde tracing combined with immunocytochemistry. *J Comp Neurol* 284: 12–35.
37. De Zeeuw CI, et al. (1998) Microcircuitry and function of the inferior olive. *Trends Neurosci* 21:391–400.
38. Van Der Giessen RS, et al. (2008) Role of olivary electrical coupling in cerebellar motor learning. *Neuron* 58:599–612.
39. Grailhe R, et al. (1999) Increased exploratory activity and altered response to LSD in mice lacking the 5-HT(5A) receptor. *Neuron* 22:581–591.
40. Lee J, Kim D, Shin HS (2004) Lack of delta waves and sleep disturbances during non-rapid eye movement sleep in mice lacking alpha1G-subunit of T-type calcium channels. *Proc Natl Acad Sci USA* 101:18195–18199.
41. Steriade M, McCormick DA, Sejnowski TJ (1993) Thalamocortical oscillations in the sleeping and aroused brain. *Science* 262:679–685.
42. McCormick DA, Bal T (1994) Sensory gating mechanisms of the thalamus. *Curr Opin Neurobiol* 4:550–556.
43. DiCarlo JJ, Lane JW, Hsiao SS, Johnson KO (1996) Marking microelectrode penetrations with fluorescent dyes. *J Neurosci Methods* 64:75–81.
44. Kim T, et al. (2004) The biochemical activation of T-type Ca2+ channels in HEK293 cells stably expressing α1G and Kir2.1 subunits. *Biochem Biophys Res Commun* 324:401–408.